

Enhancement of the effective mass at high magnetic fields in CeRhIn₅

L. Jiao,^{1,2} M. Smidman,^{1,*} Y. Kohama,³ Z. S. Wang,^{4,†} D. Graf,⁵ Z. F. Weng,¹
Y. J. Zhang,¹ A. Matsuo,³ E. D. Bauer,⁶ Hanoh Lee,¹ S. Kirchner,⁷ J. Singleton,⁸
K. Kindo,³ J. Wosnitza,⁹ F. Steglich,^{1,2} J. D. Thompson,¹⁰ and H. Q. Yuan^{1,11,‡}

¹*Center for Correlated Matter and Department of Physics,
Zhejiang University, Hangzhou, Zhejiang 310058, China*

²*Max Planck Institute for Chemical Physics of Solids, 01187 Dresden, Germany*

³*Institute for Solid State Physics, The University of Tokyo, Kashiwa, Chiba 277-8581, Japan*

⁴*Hochfeld-Magnetlabor Dresden (HLD-EMFL), Helmholtz-Zentrum Dresden-Rossendorf, D-01328 Dresden, Germany*

⁵*National High Magnetic Field Laboratory, Florida State University, Tallahassee, FL 32310*

⁶*Condensed Matter and Magnet Science, Los Alamos National Laboratory, Los Alamos, NM, USA*

⁷*Zhejiang Institute of Modern Physics, Zhejiang University, Hangzhou, Zhejiang 310027, China*

⁸*Condensed Matter and Magnet Science, Los Alamos National Laboratory, Los Alamos 87545, NM, USA*

⁹*Hochfeld-Magnetlabor Dresden (HLD-EMFL), Helmholtz-Zentrum Dresden-Rossendorf, 01328 Dresden, Germany*

¹⁰*Condensed Matter and Magnet Science, Los Alamos National Laboratory, Los Alamos 210093, NM, USA*

¹¹*Collaborative Innovation Center of Advanced Microstructures, Nanjing University, Nanjing, China*

The Kondo-lattice compound CeRhIn₅ displays a field-induced Fermi surface reconstruction at $B^* \approx 30$ T, which occurs within the antiferromagnetic state, prior to the quantum critical point at $B_{c0} \approx 50$ T. Here, in order to investigate the nature of the Fermi surface change, we measured the magnetostriction, specific heat, and magnetic torque of CeRhIn₅ across a wide range of magnetic fields. Our observations uncover the field-induced itineracy of the 4*f* electrons, where above $B_{\text{onset}} \approx 17$ T there is a significant enhancement of the Sommerfeld coefficient, and spin-dependent effective cyclotron masses determined from quantum oscillations. Upon crossing B_{onset} , the temperature dependence of the specific heat also shows distinctly different behavior from that at low fields. Our results indicate that the Kondo coupling is remarkably robust upon increasing the magnetic field. This is ascribed to the delocalization of the 4*f* electrons at the Fermi surface reconstruction at B^* .

PACS numbers: 75.30.Mb; 71.10.Hf; 74.70.Tx

I. INTRODUCTION

Kondo-lattice systems are prototypical strongly correlated materials, in which thermal and quantum fluctuations can drive the electronic states in spin, charge, or orbital channels and induce various phases. In the simplest model, the ground states of heavy-fermion compounds are determined by the competition between the Ruderman-Kittel-Kasuya-Yosida (RKKY) interaction and the Kondo effect, which evolve differently with temperature, magnetic field, and pressure¹⁻⁴. Adjusting non-thermal control parameters can tune the strengths of both the RKKY coupling, which is the intersite exchange interaction between localized moments leading to magnetic order, and the Kondo coupling corresponding to onsite antiferromagnetic exchange between localized moments and itinerant conduction electrons, giving rise to a nonmagnetic singlet ground state. To date, many novel phenomena, such as non-Fermi-liquid behavior and unconventional superconductivity, have been found in the vicinity of quantum critical points (QCPs), where the Kondo coupling prevails and the magnetic ordering temperature is smoothly suppressed to zero. However, whether a universal description of quantum critical behavior can be found still needs to be determined, and in particular it is necessary to investigate how the emergent phenomena evolve upon tuning Kondo lattice systems from localized to itinerant states.

The Kondo lattice compound CeRhIn₅ provides a good opportunity to study the change from localized to delocalized 4*f* states. In zero-field at ambient pressure, the Ce 4*f* electrons in CeRhIn₅ are localized and order antiferromagnetically at around 3.8 K⁵⁻⁷. In high magnetic fields, evidence for a field-induced spin-density-wave (SDW) type QCP has been found near the critical field $B_{c0} \approx 50$ T⁸. Theoretically, this kind of conventional SDW-type QCP involves only three-dimensional fluctuations of the antiferromagnetic (AFM) order parameter around zero temperature⁹⁻¹¹, which has been identified in some heavy-fermion compounds, such as CeCu₂Si₂¹², and La-doped CeRu₂Si₂¹³. In this scenario, the *f* electrons already are delocalized in the magnetically ordered region, and only a few “hot spots/lines” on the Fermi surface (FS) become critical at the QCP⁴. For CeRhIn₅, a field-induced change of the FS was observed inside the AFM state at around $B^* \approx 30$ T, as concluded from sharp changes in the dHvA frequencies, Hall effect, and magnetoresistance^{8,14,15}. The expansion of the FS volume (or charge carrier concentration) is attributed to the 4*f* electrons becoming delocalized at $B > B^*$ ⁸, which is consistent with the presence of a conventional SDW-type QCP at B_{c0} . Such a field-induced delocalization of the 4*f* electrons is different to that generally anticipated for Kondo lattice systems, where the 4*f* electrons are often expected to be more localized in high fields¹⁶⁻¹⁹.

To date, no clear anomalies have been detected around B^* in the specific heat⁸, torque magnetometry^{8,14}, and magnetic susceptibility²⁰. Therefore, the evolution of the Ce $4f$ electrons in high magnetic fields is still not determined, and the nature of the quantum phase transition at B^* is not well understood⁸. Moreover, evidence was recently provided for a spin nematic state in CeRhIn₅ at high fields, from resistivity measurements of microstructured devices for certain field orientations²¹. A pronounced in-plane anisotropy was found in the resistivity when a field was applied 20° away from the c axis, where the anisotropy showed a sudden increase above B^* . Obviously, the relationship between this enigmatic phase transition and the local to itinerant transition of the $4f$ electrons needs to be resolved. Here, we report a detailed study of the magnetostriction, specific heat, and de Haas-van Alphen (dHvA) effect of CeRhIn₅ in high magnetic fields. These results enable us to trace the evolution of the correlated electrons upon approaching B^* .

II. EXPERIMENTAL DETAILS

Single crystals of CeRhIn₅ were grown using In flux, as described elsewhere⁸. Measurements of the absolute values of the specific heat are extremely challenging in pulsed magnetic fields. These were performed in a long-pulsed magnet at the International Megagauss Science Laboratory of ISSP in Kashiwa up to 43.5 T. To minimize the influence associated with the field instability of the pulsed field, we generated highly stabilized (± 100 Oe) magnetic fields with a 100 ms timescale using a field-feedback controller²² and measured the absolute value of the specific heat in the stabilized field by applying the heat-pulse method²³. The resolution of the specific heat data were successfully improved²⁴, and a detailed analysis of the data is possible up to 43.5 T. The optical fibre Bragg grating (FBG) method^{25,26} was used to measure the magnetostriction in pulsed magnetic fields up to 60 T with $B \parallel a$ and $B \parallel c$. Measurements of the dHvA effect of CeRhIn₅ were conducted utilizing a torque technique between 5 K and 300 mK in dc fields up to 45 T⁸.

III. RESULTS

A. High-field magnetostriction

The magnetostriction of a metal is proportional to the conduction-electron density of states at the Fermi level²⁷. Therefore, so as to gain insights into the interactions between the conduction electrons and the lattice, we performed measurements of the longitudinal magnetostriction of CeRhIn₅ for $B \parallel a$ and $B \parallel c$ at 0.7 K, where the relative length changes $\Delta L/L$ and the corresponding field derivatives as a function of applied

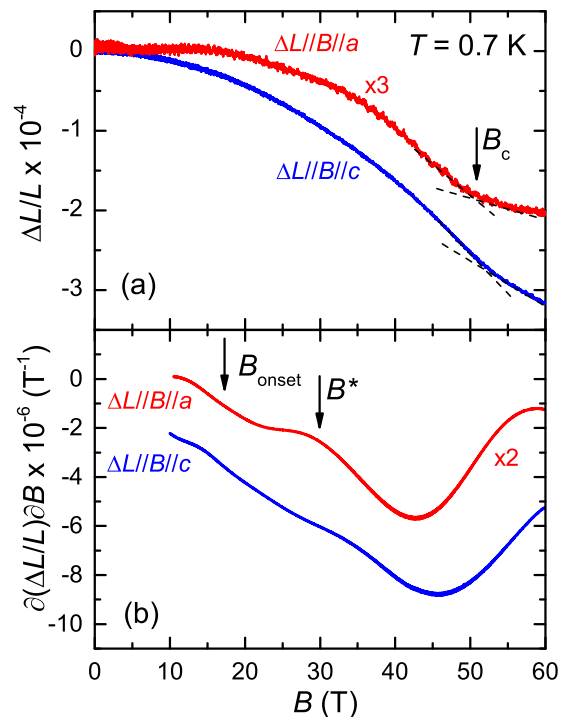


FIG. 1. Magnetostriction of CeRhIn₅ in high magnetic fields, where (a) the fractional length change $\Delta L/L$, and (b) the derivative are displayed for $B \parallel a$ and $B \parallel c$ at 0.7 K, and the former data have been scaled. The arrows mark the onset of the mass enhancement B_{onset} , B^* and the critical field B_c .

field are displayed in Fig. 1. It can be seen that at lower fields up to around 15 T, the in-plane $\Delta L/L$ is nearly field independent, before beginning to decrease more rapidly at higher fields. Meanwhile at very high fields in the vicinity of the critical field B_c , $\Delta L/L$ shows a change in slope at 50 and 52 T for fields along the a - and c -axes respectively. While no clear anomaly is observed near $B^* \approx 30$ T along the c axis, there is a kink in $\partial(\Delta L/L)/\partial B$ along the a -axis [Fig.1(b)]. These results give further evidence for the existence of B^* from in-plane measurements, but also suggest that the coupling to the lattice of the Fermi surface transition B^* is rather weak. While the critical fluctuations associated with phenomena such as CDW transitions and valence changes generally couple strongly to the lattice, those corresponding to SDW order commonly couple more weakly²⁸. We note that weak anomalies have also been reported in the magnetostriction at B^* when fields are applied at 11° and 20° to the c -axis^{21,29}. It is possible that the magnetostriction change at B^* is too weak to be resolved in our measurements with fields along the c -axis.

B. Specific heat in high magnetic fields

Figure 2(a) shows the temperature dependence of the specific heat of CeRhIn₅ [$C(T)$] at different magnetic

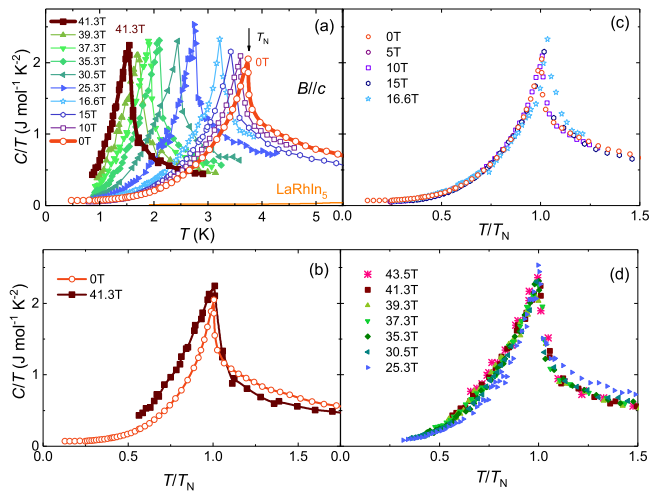


FIG. 2. (a) Temperature dependence of the specific heat C/T of CeRhIn_5 in various magnetic fields with $B \parallel c$. Data between 0–15 T were measured in a PPMS while the high-field data was measured in pulsed magnetic fields. The orange curve at low C/T is the specific heat of LaRhIn_5 at $B = 0$. (b) C/T as a function of T/T_N in zero field and 41.3 T, one field above and one below B^* . C/T is displayed as a function of T/T_N for applied fields (c) up to 16.6 T, and (d) at fields higher than 16.6 T.

fields with $B \parallel c$, reaching a higher maximum field, and lower temperatures in the high-field region than previous studies of $C(T)$ ³⁰; here the level of precision allows for a detailed study of the evolution of electronic correlations. The AFM transition is clearly observed at all fields, which is manifested by a pronounced peak in $C(T)/T$. With increasing magnetic field, T_N smoothly shifts to lower temperatures, consistent with previous reports^{8,30}. The accuracy of the current data obtained in pulsed magnetic fields was checked by comparing to those measured in dc fields^{24,30}. C/T in the displayed temperature range is much larger than in the La homologue, and therefore the phonon contribution is negligible.

Figure 2(b) displays C/T as a function of T/T_N for two representative curves [bold in Fig. 2(a)], at $B = 0$ and 41.3 T, which show distinctly different behavior. At high fields, the transition is sharper, with a larger jump, while the values of C/T just above T_N are reduced. This suggests that compared to the low-field results, at high fields there is a reduction in the contribution from short-range fluctuations which appear above the magnetic ordering temperature. In Fig. 2(c), C/T is displayed for fields up to 16.6 T as a function of T/T_N ²⁴. One can see that the data below T_N overlap fairly well, demonstrating that T_N is the only energy scale which determines the specific heat in this field range. On the other hand, the higher field data do not scale so well as a function of T/T_N , suggesting the role of additional parameters. This may also be taken as an indication of changes in the underlying correlated state, such as a variation of the effective mass, as described below.

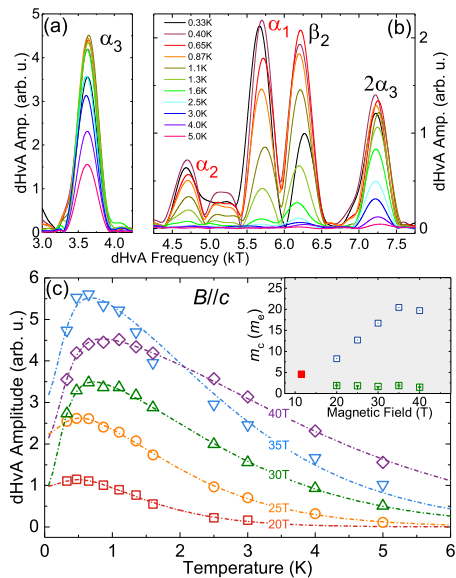


FIG. 3. (a) and (b) FFT spectra of dHvA effect oscillations of CeRhIn_5 for the field range 35–45 T at various temperatures with for $B \parallel c$. (c) Temperature dependence of dHvA oscillation amplitudes of the α_3 orbit at various magnetic fields. The field values correspond to the midpoints of the 10 T wide field windows used in the FFT. The dashed lines display fits to the spin-dependent LK formula. The inset shows the field dependence of the cyclotron masses of the two spin orientations (open blue and green squares). Experimental data obtained at low magnetic fields from Refs. 32 and 33 are also shown by the red solid squares.

We further analyzed the data well below T_N using $C/T = \gamma + C_m/T$, where γ is the Sommerfeld coefficient, and C_m is the contribution of the AFM magnons to the specific heat^{24,31}. This equation can be fitted well to the low-temperature data [$T < 0.7T_N$] below 35.3 T. Above 35.3 T, the fit is less reliable due to the limited accessible data for $T < 0.7T_N$. A detailed discussion of the specific heat fits is presented in the Supplemental Material²⁴, where with increasing magnetic field, $\gamma(B)$ changes little at lower fields, but shows an enhancement onset at fields above $B_{\text{onset}} \approx 17$ T.

C. Analysis of the effective cyclotron masses from the dHvA effect

To directly probe the effective mass of the charge carriers, we also measured the dHvA effect. It has been established by band-structure calculations and quantum-oscillation measurements that the FS of CeRhIn_5 primarily arises from three bands (α, β, γ), where the dHvA effect is dominated by the extremal orbits denoted $\alpha_1, \alpha_2, \alpha_3, \beta_1$, and β_2 ^{6,33}. In our previous work (Refs. 8 and 15), we studied the magnetic field dependence of the dHvA frequencies at 0.33 K, which yielded clear evidence for an abrupt expansion of the FS volume at B^* . Here,

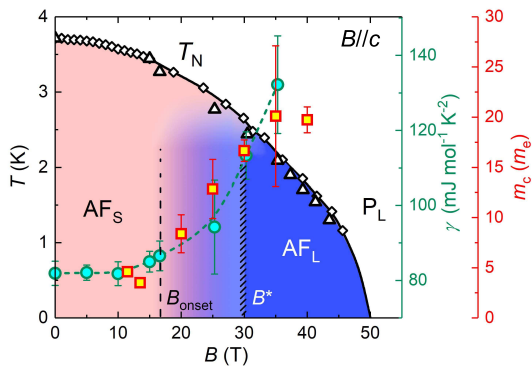


FIG. 4. Temperature-field phase diagram of CeRhIn₅ where the field dependence of γ and the effective mass, m_c , of the heavy spin orientation of the FS sheet for $B \parallel c$ [see inset of Fig. 3(c)] are shown by the olive circles and red squares respectively. The scales for these quantities with corresponding colors are on the right side of the panel. The positions of the FS reconstruction (B^*) and the field at which the effective mass enhancement onsets (B_{onset}) are also displayed. The triangular and diamond shaped symbols represent T_N as obtained here and in Ref. 8, respectively.

we further investigate the temperature and magnetic-field dependence of the dHvA amplitudes, from which the effective cyclotron masses of the charge carriers are determined, focussing on the α_3 orbit, which corresponds to the strongest oscillation.

In a conventional metal, the dHvA oscillation amplitudes are given by the Lifshitz–Kosevich (LK) formula³⁴, where in the nonspin-dependent case the temperature and field dependence are determined by two adjustable parameters, the effective cyclotron mass (m_c) and the Dingle temperature (T_D), the analysis of the latter being presented in the Supplemental Material²⁴. Figures 3(a) and (b) display the fast Fourier transform (FFT) spectra of the dHvA oscillations of CeRhIn₅ at various temperatures for $35 \text{ T} \leq B \leq 45 \text{ T}$ with $B \parallel c$. If the data were well described by the LK formula, the amplitude of the oscillations would monotonically increase with decreasing temperature. As shown in Fig. 3, this is the case for the α_3 orbit above 1 K only, but below this temperature the dHvA amplitude reaches a maximum before it decreases with decreasing temperature. This decrease cannot arise due to an increased scattering rate, since it is found that T_D decreases strongly in this temperature and magnetic field range²⁴. Such a phenomenon was previously observed in a pulsed-field experiment in the range 31–50 T and was attributed to the formation of SDW order³². However, this explanation cannot account for the similar observations of the α_3 orbit of CeCoIn₅, where it was ascribed to spin-dependent mass enhancements of the FS³⁵. This phenomenon may arise in heavy fermion systems when a sufficiently high magnetic field lifts the spin degeneracy of the renormalized bands by the Zeeman effect. Due to the asymmetry of the electronic bands near the Fermi level in

the heavy fermion state, this can lead to different effective masses for the two spin species³⁵. Therefore, we studied the spin-dependent effective masses of the electrons on the α_3 orbit by performing FFT on the dHvA oscillations at various temperatures in 10 T intervals.

Following Refs. 35 and 36, a spin-dependent LK formula was used to fit the derived amplitudes given by $\tilde{M} = \sqrt{(\tilde{M}_\uparrow + \tilde{M}_\downarrow)^2 \cos^2 \theta + (\tilde{M}_\uparrow - \tilde{M}_\downarrow)^2 \sin^2 \theta}$, where θ is the phase term and \tilde{M}_\uparrow (\tilde{M}_\downarrow) is the dHvA amplitude of the spin up (down) FS described by the LK formula. This model fits the experimental results well [dashed-dotted lines in Fig. 3(c)]. As shown in the inset of Fig. 3(c), the fit reveals a relatively large field-dependent effective mass for one of the spin orientations but a small, nearly field-independent mass for the other one. It should be noted that we cannot determine which spin orientation corresponds to the carriers with the larger effective mass. The mass of the lighter band is around $1.6m_e$ in the measured field range, which is slightly larger than for the corresponding orbit in LaRhIn₅⁶, while the mass of the heavier band increases with increasing magnetic field. Note that this mass reaches a value of about $20m_e$ when the midpoint field is 35 T, at which the dHvA amplitude displays a significantly steeper temperature dependence. Such a heavy mass at a field above B^* is similar to that of the corresponding orbit of CeCoIn₅³⁵, where the $4f$ electrons also contribute to the Fermi surface⁷. A similar suppression of the dHvA amplitude at low temperatures is observed for the β_2 orbit²⁴. Since dHvA signals of the α_2 , α_1 , and β_1 orbits only appear below 2.5 K and above 30 T, the field dependences of these cyclotron masses cannot be estimated.

IV. DISCUSSION

Our main results are summarized in Fig. 4, which show that although T_N is smoothly suppressed as a function of applied field, there is an enhancement of the γ coefficient and effective cyclotron mass m_c which onsets above $B_{\text{onset}} \approx 17$ T, well below $B^* \approx 30$ T. Combined with our previous results^{8,14,15}, we are able to identify a number of distinct behaviors across different field ranges at low temperature. Between zero field and B^* , the $4f$ electrons are well localized and the Fermi surface is small. At lower fields up to B_{onset} , γ barely changes with increasing field, and there is also little change in the in-plane magnetostriction. However, upon further increasing the field, the specific heat and dHvA measurements are consistent in revealing a clear enhancement of the effective quasiparticle mass, which likely signals an increasing fraction of the large FS in the fluctuation spectrum of the FS crossover³⁷. We note that an anomaly at $B_M \approx 18$ T was previously found in Hall-resistivity measurements⁸, but whether this is related to the onset of the electronic mass enhancement requires further determination. At the subsequent

crossover at $B^* \approx 30$ T, the Fermi surface becomes reconstructed from small to large. Here, a maximum of the effective mass at ≈ 30 T may be anticipated, corresponding to the finite-temperature signature of a zero-temperature divergence⁴. However, it is difficult to confirm whether such a maximum occurs, due to the extremely large error bar of the cyclotron mass for the field-window centered around 35 T, in comparison to the preceding and following data points at 30 T and 40 T, respectively. It can be seen in Fig. 3(c) that the 35 T data shows the steepest increase with decreasing temperature and is less well described by the LK-formula for spin-dependent cyclotron masses, consistent with a rapid field-induced change of the electronic structure in this field-window. On the other hand, the absence of such a maximum might be related to there being a sizeable mass enhancement only for *one* spin orientation. The high-field mass enhancement significantly affects $C(T)$, where the analysis of the low-temperature data suggests a pronounced weakening of the RKKY coupling strength above B_{onset} ²⁴. In addition, the short-ranged correlations above T_N appear to be substantially reduced, although the magnetic structure likely remains unchanged to fields above B^* ³⁸.

The field-induced increase of the effective mass, together with the observed changes to $C(T)$ in the magnetic state and the drastic changes of some dHvA frequencies upon crossing B^* with others remaining at a nearly constant value⁸, implies that the Fermi surface reconstruction is driven by the delocalization of the $4f$ electrons. Whether this delocalization transition occurs as an orbitally selective Mott transition or other forms of Kondo destruction is an interesting open question. Addressing it may require relating the observed changes of certain dHvA frequencies to details of the Fermi surface, and thus disentangling the effects of the f -electron degrees of freedom, momentum dependence of the hybridization and band structure of the conduction electrons. This may shed new light on how orbital and spin degrees of freedom are entangled in strong magnetic fields. Recent results indicating the emergence of an anisotropy of the electrical resistivity due to spin nematicity²¹ at $B \approx B^*$ in CeRhIn₅ also show a close relationship to the SDW phase with itinerant $4f$ electrons. Indeed, in the low-field regime no resistivity anisotropy is observed but at intermediate fields *below* 30 T, there is an onset of this resistivity anisotropy near B_{onset} ²⁴. This in turn suggests that the presence

of itinerant, rather than localized, $4f$ -electron states is related to the emergence of this new electronic (nematic) order.

V. SUMMARY

To conclude, we have probed the nature of the Fermi surface reconstruction associated with the abrupt change of the Fermi surface volume of CeRhIn₅ at $B^* \approx 30$ T. We find a field-induced enhancement of the effective mass which onsets at $B_{\text{onset}} \approx 17$ T and significantly increases with increasing field below B^* , as well as distinct changes to the temperature dependence of the specific heat. These new insights into the Fermi surface reconstruction which takes place inside the magnetically ordered states of the Kondo-lattice system CeRhIn₅ should be relevant to other heavy-fermion compounds, as well as a broader range of correlated metals in proximity to Mott insulating states, such as high- T_c cuprates or organic charge-transfer salts.

ACKNOWLEDGMENTS

We acknowledge valuable discussions with S. Arsenijevic, P. J. W. Moll, Q. Si, F. Ronning, S. Paschen, O. Stockert and C.-L. Huang. Work at Zhejiang University was supported by the National Natural Science Foundation of China (Grants No. U1632275 and No. 11474250), National Key R&D Program of China (Grants No. 2017YFA0303100 and No. 2016YFA0300202), and the Science Challenge Project of China (No. TZ2016004). Work at Los Alamos National Laboratory was performed under the auspices of the US Department of Energy (DoE). A portion of this work was performed at the National High Magnetic Field Laboratory, which is funded by the National Science Foundation through DMR-1157490 and the US Department of Energy and the State of Florida. J. S. appreciates funding from Basic Energy Sciences, U. S. Department of Energy FWP *Science in 100 T* program. We acknowledge the support of the HLD at HZDR, member of the European Magnetic Field Laboratory (EMFL), and support by the ANR-DFG grant Fermi-NESt. L.J. acknowledges support by the Alexander-von-Humboldt foundation.

* mmsmidman@zju.edu.cn

† Present address: High Magnetic Field Laboratory of the Chinese Academy of Sciences, Hefei 230031, China

‡ hqyuan@zju.edu.cn

¹ G. R. Stewart, Non-Fermi-liquid behavior in d - and f -electron metals. Rev. Mod. Phys. **73**, 797 (2001).

² H.v. Löhneysen, A. Rosch, M. Vojta, and P. Wölfle, Fermi-liquid instabilities at magnetic quantum phase transitions. Rev. Mod. Phys. **79**, 1015 (2007).

³ Z. F. Weng, M. Smidman, L. Jiao, X. Lu, and H. Q. Yuan, Multiple quantum phase transitions and superconductivity in Ce-based heavy fermions. Rep. Prog. Phys. **79**, 094503 (2016).

- ⁴ P. Gegenwart, Q. Si, F. Steglich, Quantum criticality in heavy-fermion metals. *Nat. Phys.*, **4**, 186 (2008).
- ⁵ H. Hegger, C. Petrovic, E. G. Moshopoulou, M. F. Hundley, J. L. Sarrao, Z. Fisk, and J. D. Thompson, Pressure-induced superconductivity in quasi-2D CeRhIn₅. *Phys. Rev. Lett.* **84**, 4986 (2000).
- ⁶ H. Shishido, R. Settai, D. Aoki, S. Ikeda, H. Nakawaki, N. Nakamura, T. Iizuka, Y. Inada, K. Sugiyama, T. Takeuchi, K. Kindo, T. C. Kobayashi, Y. Haga, H. Harima, Y. Aoki, T. Namiki, H. Sato, and Y. Ōnuki, Fermi Surface, Magnetic and Superconducting properties of LaRhIn₅ and CeTIn₅ (T: Co, Rh and Ir). *J. Phys. Soc. Jpn.* **71**, 162 (2002).
- ⁷ N. Harrison, U. Alver, R. G. Goodrich, I. Vekhter, J. L. Sarrao, P. G. Pagliuso, N. O. Moreno, L. Balicas, Z. Fisk, D. Hall, Robin T. Macaluso, and Julia Y. Chan, 4f-electron localization in Ce_xLa_{1-x}MIn₅ with M=Co, Rh, or Ir. *Phys. Rev. Lett.* **93**, 186405 (2004).
- ⁸ L. Jiao, Y. Chen, Y. Kohama, D. Graf, E. D. Bauer, J. Singleton, J. Zhu, Z. Weng, G. Pang, T. Shang, J. Zhang, H. Lee, T. Park, M. Jaime, J. D. Thompson, F. Steglich, Q. Si, and H. Q. Yuan, Fermi surface reconstruction and multiple quantum phase transitions in the antiferromagnet CeRhIn₅. *Proc. Natl. Acad. Sci. U.S.A.*, **112**, 673 (2015).
- ⁹ J. A. Hertz, Quantum critical phenomena. *Phys. Rev. B* **14**, 1165 (1976).
- ¹⁰ T. Moriya, Spin Fluctuations in Itinerant Electron Magnetism (Springer, Berlin, 1985).
- ¹¹ A. J. Millis, Effect of a nonzero temperature on quantum critical points in itinerant fermion systems. *Phys. Rev. B* **48**, 7183 (1993).
- ¹² J. Arndt, O. Stockert, K. Schmalzl, E. Faulhaber, H.S. Jeevan, C. Geibel, W. Schmidt, M. Loewenhaupt, and F. Steglich, Spin fluctuations in normal state CeCu₂Si₂ on approaching the quantum critical point. *Phys. Rev. Lett.* **106**, 246401 (2011).
- ¹³ S. Kambe, S. Raymond, L. Regnault, J. Flouquet, P. Lejay, and P. Haen, Application of the SCR spin fluctuation theory for the magnetic instability in heavy fermion system Ce_{1-x}La_xRu₂Si₂. *J. Phys. Soc. Jpn.* **65**, 3294 (1996).
- ¹⁴ P. J. W. Moll, B. Zeng, L. Balicas, S. Galeski, F. F. Balakirev, E. D. Bauer, and F. Ronning, Field-induced density wave in the heavy-fermion compound CeRhIn₅. *Nat. Commun.* **6**, 6663 (2015).
- ¹⁵ L. Jiao, Z. F. Weng, M. Smidman, D. Graf, J. Singleton, E. D. Bauer, J. D. Thompson, and H. Q. Yuan, Magnetic field-induced Fermi surface reconstruction and quantum criticality in CeRhIn₅. *Phil. Mag.* **97**, 3446-3459 (2017).
- ¹⁶ H. Aoki, S. Uji, A. K. Albessard, and Y. Ōnuki, Transition of f electron nature from itinerant to localized: Metamagnetic transition in CeRu₂Si₂ studied via the de Haas-van Alphen effect. *Phys. Rev. Lett.* **71**, 2110 (1993).
- ¹⁷ N. Harrison, P. Meeson, P. -A. Probst and M. Springford, Quasiparticle and thermodynamic mass in the heavy-fermion system CeB₆. *J. Phys. Condens. Matter* **5**, 7435 (1993).
- ¹⁸ N. Harrison, D. W. Hall, R. G. Goodrich, J. J. Vuillemin, and Z. Fisk, Quantum Interference in the Spin-Polarized Heavy Fermion Compound CeB₆: Evidence for Topological Deformation of the Fermi Surface in Strong Magnetic Fields. *Phys. Rev. Lett.* **81**, 870 (1998).
- ¹⁹ P. C. Ho, J. Singleton, P. A. Goddard, F. F. Balakirev, S. Chikara, T. Yanagisawa, M. B. Maple, D. B. Shrekenhamer, X. Lee, and A. T. Thomas, Fermi surface topologies and low-temperature phases of the filled skutterudite compounds CeOs₄Sb₁₂ and NdOs₄Sb₁₂. *Phys. Rev. B* **94**, 205140 (2016).
- ²⁰ T. Takeuchi, T. Inoue, K. Sugiyama, D. Aoki, Y. Tokiwa, Y. Haga, K. Kindo, and Y. Ōnuki, Magnetic and Thermal Properties of CeIrIn₅ and CeRhIn₅. *J. Phys. Soc. Jpn.* **70**, 877 (2001).
- ²¹ F. Ronning, T. Helm, K. R. Shirer, M. D. Bachmann, L. Balicas, M. K. Chan, B. J. Ramshaw, R. D. McDonald, F. F. Balakirev, M. Jaime, E. D. Bauer and P. J. W. Moll, Electronic in-plane symmetry breaking at field-tuned quantum criticality in CeRhIn₅. *Nature* **548**, 313-317 (2017)
- ²² Y. Kohama and K. Kindo, Generation of flat-top pulsed magnetic fields with feedback control approach. *Rev. Sci. Instrum.* **86**, 104701 (2015).
- ²³ Y. Kohama, Y. Hashimoto, S. Katsumoto, M. Tokunaga, and K. Kindo, Heat-pulse measurements of specific heat in 36 ms pulsed magnetic fields. *Meas. Sci. Technol.* **24**, 115005 (2013).
- ²⁴ See Supplemental Material for further information about the experimental methods, the specific heat fitting, Dingle temperature analysis and a comparison between these results and the field-temperature phase diagram.
- ²⁵ R. Daou, F. Weickert, M. Nicklas, F. Steglich, A. Haase, and M. Doerr, High resolution magnetostriction measurements in pulsed magnetic fields using fiber Bragg gratings. *Rev. Sci. Instrum.* **81**, 033909 (2010).
- ²⁶ M. Rotter, Z. S. Wang, A. T. Boothroyd, D. Prabhakaran, A. Tanaka, and M. Doerr, Mechanism of spin crossover in LaCoO₃ resolved by shape magnetostriction in pulsed magnetic fields. *Sci. Rep.* **4**, 7003 (2014).
- ²⁷ N. Ekrem, A. Olabi, T. Prescott, A. Rafferty, and M. Hashmi, An overview of magnetostriction, its use and methods to measure these properties. *Mat. Proc. Techn.* **191**, 96 (2007).
- ²⁸ U. Stockert, N. Leps, L. Wang, G. Behr, S. Wurmehl, B. Büchner, and R. Klingeler, Pr magnetism and its interplay with the Fe spin-density wave in PrFeAsO_{1-x}F_x (x=0,0.15). *Phys. Rev. B* **86**, 144407 (2012).
- ²⁹ P. F. S. Rosa, S. M. Thomas, F. F. Balakirev, E. D. Bauer, R. M. Fernandes, J. D. Thompson, F. Ronning, M. Jaime, Enhanced hybridization sets the stage for electronic nematicity in CeRhIn₅. *Phys. Rev. Lett.* **122**, 016402 (2019).
- ³⁰ J. S. Kim, J. Alwood, G. R. Stewart, J. L. Sarrao, J. D. Thompson, Specific heat in high magnetic fields and non-Fermi-liquid behavior in CeMIn₅ (M=Ir,Co). *Phys. Rev. B* **64**, 134524 (2001).
- ³¹ M. A. Continentino, S. N. D. Medeiros, M. T. D. Orlando, M. B. Fontes, and E. M. Baggio-Saitovitch, Anisotropic quantum critical behavior in CeCoGe_{3-x}Si_x. *Phys. Rev. B* **64**, 012404 (2001).
- ³² A. L. Cornelius, A. J. Arko, J. L. Sarrao, M. F. Hundley, and Z. Fisk, Anisotropic electronic and magnetic properties of the quasi-two-dimensional heavy-fermion antiferromagnet CeRhIn₅. *Phys. Rev. B* **62**, 14181 (2000).
- ³³ D. Hall, E. C. Palm, T. P. Murphy, S. W. Tozer, C. Petrovic, E. Miller-Ricci, L. Peabody, C. Q. H. Li, U. Alver, R. G. Goodrich, J. L. Sarrao, P. G. Pagliuso, J. M. Wills, and Z. Fisk, Electronic structure of CeRhIn₅: de Haas-van Alphen and energy band calculations. *Phys. Rev. B* **64**, 064506 (2001).

- ³⁴ D. Shoenberg, *Magnetic Oscillations in Metals* (Cambridge University Press, 1984).
- ³⁵ A. McCollam, S. R. Julian, P. M. C. Rourke, D. Aoki, and J. Flouquet, Anomalous de Haas–van Alphen Oscillations in CeCoIn₅. *Phys. Rev. Lett.* **94**, 186401 (2005).
- ³⁶ M. Takashita, H. Aoki, T. Terashima, S. Uji, K. Maezawa, R. Settai, and Y. Ōnuki, dHvA Effect Study of Metamagnetic Transition in CeRu₂Si₂ II-The State above the Metamagnetic Transition. *J. Phys. Soc. Jpn.* **65**, 515 (1996).
- ³⁷ S. Paschen, S. Friedemann, S. Wirth, F. Steglich, S. Kirchner, and Q. Si, Kondo destruction in heavy fermion quantum criticality and the photoemission spectrum of YbRh₂Si₂. *J. Magn. Magn. Mater.* **400**, 17 (2016).
- ³⁸ G. Lesseux, T. Hattori, H. Sakai, Y. Tokunaga, S. Kambe, P. Kuhns, A. Reyes, P. Pagliuso, R. Urbano, Poster presentation, International Conference on Strongly Correlated Electron Systems, Prague, (2017.07.17-21).